A parametric study on factors influencing the onset and propagation of aortic dissection using the extended finite element method

J. Brunet, B. Pierrat, and P. Badel

Abstract*—*Objective: **Aortic dissection is a life-threatening event which starts most of the time with an intimal tear propagating along the aortic wall, while blood enters the medial layer and delaminates the medial lamellar units. Studies investigating the mechanisms underlying the initiation sequence of aortic dissection are rare in the literature, the majority of studies being focused on the propagation event. Numerical models can provide a deeper understanding of the phenomena involved during the initiation and the propagation of the initial tear, and how geometrical and mechanical parameters affect this event. In the present paper, we investigated the primary factors contributing to aortic dissection.** ***Methods:*** **A two-layer arterial model with an initial tear was developed, representing three different possible configurations depending on the initial direction of the tear. Anisotropic damage initiation criteria were developed based on uniaxial and shear experiments from the literature to predict the onset and the direction of crack propagation. We used the XFEM-based cohesive segment method to model the initiation and the early propagation of the tear along the aorta. A design of experiment was used to quantify the influence of 7 parameters reflecting crack geometry and mechanics of the wall on the critical pressure triggering the dissection and the directions of propagation of the tear.** ***Results:*** **The results showed that the obtained critical pressures (mean range from 206 to 251 mmHg) are in line with measurement from the literature. The medial tensile strength was found to be the most influential factor, suggesting that a medial degeneration is needed to reach a physiological critical pressure and to propagate a tear in an aortic dissection. The geometry of the tear and its location inside the aortic wall were also found to have an important role not only in the triggering of tear propagation, but also in the evolution of the tear into either aortic rupture or aortic dissection. A larger and deeper initial tear increases the risk of aortic dissection.** ***Conclusion:*** **The numerical model was able to reproduce the behaviour of the aorta during the initiation and propagation of an aortic dissection. In addition to confirm multiple results from the literature, different types of tears were compared and the influence of several geometrical and mechanical parameters on the critical pressure and direction of propagation was evaluated with a parametric study for each tear configuration.** ***Significance:*** **Although these results should be experimentally validated, they allow a better understanding of the phenomena behind aortic dissection and can help in improving the diagnosis and treatment of this disease.**

***Index Terms*—Aortic dissection, Finite element model, fracture, tear propagation, XFEM**

I. Introduction

AORTIC dissection is a sudden and life-threatening delamination event of the aortic wall, with an incidence of 3-35 cases per 100,000 per year, which requires rapid diagnosis and decision-making [1]. The mechanical sequence of aortic dissection can be divided into two different events: initiation and propagation. In the majority of cases, aortic dissection initiates with an intimal tear which, then, propagates and allows the blood to flow in the aortic wall creating a false lumen [2]. According to Thubrikar et al. [3], 80% of intimal tears are in the transverse direction whereas 20% are the in longitudinal direction, with the former usually involving more than half of the lumen. Another mechanism leading to aortic dissection is intramural haemorrhage caused by a rupture in the vasa vasorum [4] or by a micro-intimal tear [5]. Although this scenario is reported to be less common (4%-12%) [6], the intimal tear may be secondary to the intramural tear [7], [8]. A tear occurs when the biomechanical stress exceeds the local resistance of the wall [9]. The pressure and wall shear stress of the fluid contribute to the internal stresses in the wall. Using computational fluid dynamics, Chi et al. [10] have shown that the location of intimal tear corresponds to the area of maximum wall shear stress. Therefore, the formation of the tear appears to be a fatigue process. However, according to Carson et al. [11], the peak pressure to initiate the propagation of the dissection is a non-physiological blood pressure suggesting that abnormal blood pressure or medial degeneration compromising aortic integrity is necessary to create an aortic dissection [12]–[14]. The tear size can vary from less than 1 cm [15], [16] to several centimeters [17]. In some cases, the intimal tear does not propagate or propagates to a limited extend, this phenomenon is called subtle-discrete aortic dissection [8]. However, it should be noted that such reports of tear size and geometry refer to already extended tears (hence advanced dissection) that can be observed during surgery or imaging examinations.

The propagation of the initial tear was investigated in multiple experimental studies. For instance, liquid infusion test was used to investigate the influence of different parameters on tear propagation [12]. Tam et al. [18] showed that the pressure required to propagate dissection is negatively correlated with the depth of the tear. Using tension-inflation in an *ex-vivo* model of aortic dissection associated with a pulsatile pump mimicking blood flow, [19] found that geometrical factors of the entrance tear have a significant effect on the propagation of aortic dissection. Recently, shear stress has been identified

J. Brunet, B. Pierrat, and P. Badel are with Mines Saint-Etienne, Univ Lyon, Univ Jean Monnet, INSERM, U 1059 Sainbiose, Centre CIS, F - 42023 Saint-Etienne France, Corresponding author: jo.brunet73@gmail.com

as a possible determining factor in the initiation of aortic dissection [20], [20]. The ultimate shear stresses of the aorta in the different directions were quantified by Sommer et al. [21] by performing triaxial shear test. In a computational study, Brunet et al. [22] used a finite element model to simulate the failure of medial aortic specimens during uniaxial tensile tests. The results suggested that shear delamination strength, reduced by a local wall defect, could play a substantial role in the initiation of aortic dissection. Peeling tests were used to control the rupture and to assess the energy release rate required to propagate the dissection [23]–[26]. This mechanical test was simulated in multiple computational studies [26]–[29]. In addition to accurately modelling the peel test response, these numerical studies highlighted the importance of radially-running fibres in interlamellar strength and shear mode (mode II) in the failure process. Other studies have modelled the propagation of aortic dissection in real or idealized geometry using different approaches, for instance crack phase-field modelling [30], constrained mixture theory [31], or extended finite element method (XFEM) [32], [33]. The XFEM has been used in the present work because it allows the simulation of crack initiation and propagation along an arbitrary path without the requirement of remeshing. For more information on mechanical testing and modelling literature on aortic dissection, see Brunet et al. [34].

In the absence of external load, the aortic wall is not stress-free. If an unloaded aorta is cut radially and transected longitudinally, an opening angle and retraction, respectively, can be observed [35]. Under physiological conditions, the residual stress present in the aorta reduces the transmural stress gradient and contributes to the homeostatic state [36], [37]. In a numerical study [32], it was shown that residual stress protects the aorta from tear propagation; however, only the circumferential residual stress, not the axial pre-stretch, was considered in this study.

In most of the studies presented above, the orientation of the initial tear was assumed to be either in the tangential plane [32], longitudinal-radial plane [20], or transverse plane [30]. Nevertheless, to the authors' knowledge, there was no investigation in the literature comparing the different orientations of the tears and quantifying their effect on initiation and propagation. For this purpose, a numerical study is proposed involving a computational model of a tension-inflation test on an aortic segment with idealized geometry. Three different cases of tear orientation present in the medial layer and their propagation were simulated using XFEM. A numerical design of experiment (DoE) was used to perform a sensitivity analysis on the influence of different key parameters on the pressure required to propagate the tear and the direction of tear propagation. The objective was to determine the most influential factors in the propagation of an aortic dissection in order to better assess the patient at risk.

II. Materials and methods

This section presents the finite element model of the aortic segment with an initial tear, and the DoE approach used in this study.

A. Geometry

The geometry was composed of a two-layer cylinder with a length of 20 mm and a luminal radius of $r_i = 10$ mm in the *in vivo* state (Figure 2) [37]. The initial diameter and initial layer thicknesses of the model were calculated in each simulation to obtain the same diameter ($r_i = 10$) and thicknesses ($T_m = 1.44$ and $T_a = 0.36$) in the zero-pressure, initially stressed state. The intima was not considered in this model because it was assumed that it does not contribute significantly to the aortic wall mechanics. The medial layer and the adventitial layer were defined as 80% and 20% of the total aortic wall thickness, respectively [38]. The medial and adventitial thicknesses are listed in Table I.

As demonstrated by Holzapfel et al. [36], the aorta is subjected to a complex three-dimensional residual stress state under *in vivo* conditions. To account for the physiologically present residual stress in the aortic wall, the geometry was modelled with an opening angle α. Although the opening angles of the intima, media, and adventitia are different, a unique opening angle was taken for the entire model for the sake of simplicity. An axial pre-stretch was also applied to the model during the simulation to account for the residual longitudinal stretch present under physiological conditions (see Section II-D).

The aorta was meshed with 58500 C3D8H elements in Abaqus based on a mesh sensitivity analysis previously performed on the critical pressure to ensure that the influence of the mesh size on the results was negligible (see Supplementary Material). Hybrid elements were used to ensure incompressibility and avoid volumetric locking. A tear was modelled as a surface in the aortic media - disconnecting adjacent elements - to initiate aortic dissection. Three different types of tear, presented in Figure 1, were modelled. The tears were named according to the plane in which they were located: a θ-z tear is a tear in the circumferential-longitudinal plane, a r-z tear is a tear in the radial-longitudinal plane, and a r-θ tear is a tear in the radial-circumferential plane. These different cases correspond to the different initial tear geometries seen in the literature [3], [18].

	Thickness (mm)	μ (MPa)	k_1 (MPa)	k_2 (-)	γ (°)	κ (-)
Media	1.44	0.032	0.09	19.0	41.6	0.12
Adventitia	0.36	0.027	0.37	15.2	54.8	0.25

TABLE I: Thickness and elastic constitutive parameters of the numerical model of the aortic wall layers, obtained from the literature [38], [39]

B. Elastic constitutive model

The aortic wall was modelled with the Gasser-Holzapfel-Ogden (GHO) hyperelastic model. The material was assumed fully incompressible. A multiplicative split of the strain–energy function into a volumetric and a deviatoric

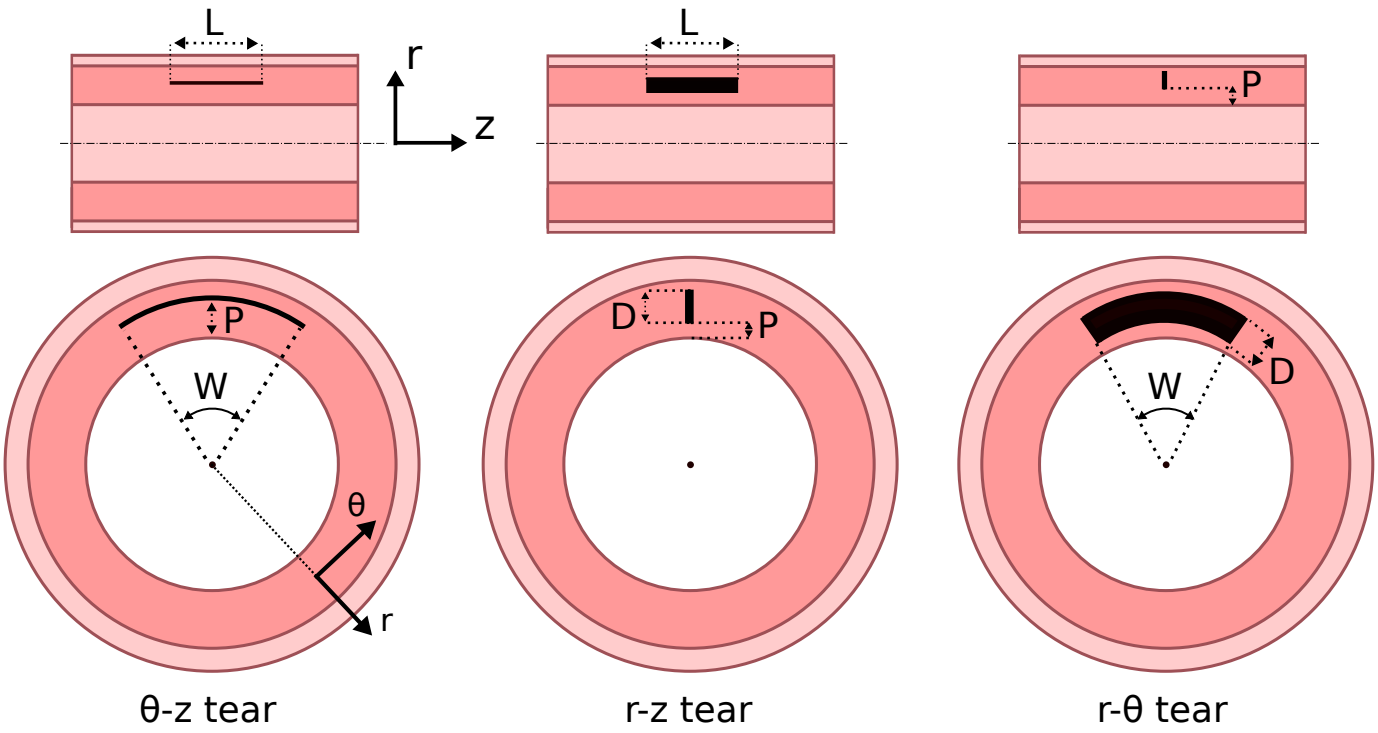

Fig. 1: The three tear configurations with the parameters defining each tear: P is the position of the tear in the radial direction, W is the width of the tear, L is the length of the tear, and D is the depth of the tear. The tears are named according to the plane in which they were located.

part was performed to ensure incompressibility. For further information on the theory behind this model see Holzapfel [40]. The isochoric strain energy function is composed of an isotropic neo-Hookean term $\bar{\psi}_m$, representing the ground matrix and the elastin fibres, and anisotropic terms $\bar{\psi}_f$, accounting for two families of collagen fibres symmetrically arranged [41]. The model was extended to account for the dispersion of collagen fibres [42]. The isochoric strain energy function is defined as :

$$\bar{\psi} = \bar{\psi}_m + \bar{\psi}_f, \tag{1}$$

with the isotropic term defined as

$$\bar{\psi}_m = \frac{\mu}{2}(\bar{I}_1 - 3), \tag{2}$$

where μ denotes the neo-Hookean parameter and $\bar{I}_1 = tr(\bar{C})$ is the first invariant of the deviatoric right Cauchy-Green tensor $\bar{C}$ (with $\bar{C} = \bar{F}^T\bar{F}$ and $F = J^{\frac{1}{3}}\bar{F}$). The anisotropic terms are defined as

$$\bar{\psi}_{f,i} = \frac{k_1}{2k_2}[e^{(k_2(\bar{I}_i^* - 1)^2)} - 1], \tag{3}$$

with

$$\bar{I}_i^* = \kappa\bar{I}_1 + (1 - 3\kappa)\bar{I}_i, \quad i = 4, 6, \tag{4}$$

where $i = 4$ and $i = 6$ correspond to the two families of fibres. $\bar{I}_4 = \bar{C} : M \otimes M$ and $\bar{I}_6 = \bar{C} : M' \otimes M'$ are the two modified pseudo-invariants and are equal to the square of the stretch of the fibres initially oriented along M and M'. These vectors are symmetric with respect to the longitudinal direction of the aorta, their direction is defined with respect to the circumferential direction with an angle γ (Figure 2). γ and κ are, respectively, the mean orientation of the fibres and the parameter accounting for their dispersion. k_1, k_2 are material parameters determined by mechanical testing. The constitutive parameters were taken from [39]. They are reported in Table I.

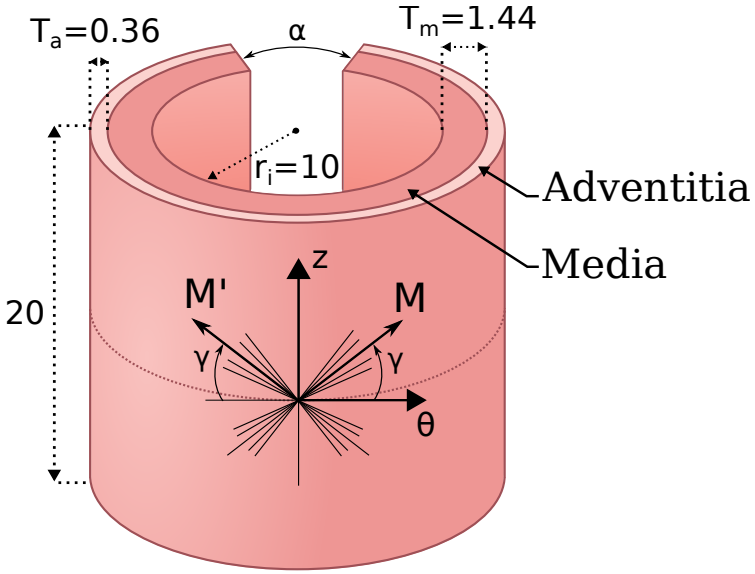

Fig. 2: Geometry of the aortic segment used in the numerical model. All dimensions are in millimeters.

C. Failure criteria

The mechanical behaviour of the aorta is anisotropic: this is the case not only with the elastic constitutive behaviour but also with the tensile and shear strengths, which vary according to the direction. Hence, four failure criteria were created with an associated direction of crack propagation (Eq 6, 7, 8, 9).

The Cauchy stress tensor was defined by

$$\sigma = \begin{bmatrix} \sigma_{rr} & \sigma_{r\theta} & \sigma_{rz} \\ \sigma_{r\theta} & \sigma_{\theta\theta} & \sigma_{\theta z} \\ \sigma_{rz} & \sigma_{\theta z} & \sigma_{zz} \end{bmatrix}, \tag{5}$$

and the failure criteria were

Radial failure criterion :

$$\sqrt{(\frac{\sigma_{rr}}{T_r})^2 + (\frac{\sigma_{r\theta}}{S_{r\theta}})^2 + (\frac{\sigma_{rz}}{S_{rz}})^2} = 1, \tag{6}$$

Circumferential failure criterion :

$$\sqrt{(\frac{\sigma_{\theta\theta}}{T_\theta})^2 + (\frac{\sigma_{r\theta}}{S_{r\theta}})^2 + (\frac{\sigma_{\theta z}}{S_{\theta z}})^2} = 1, \tag{7}$$

Longitudinal failure criterion :

$$\sqrt{(\frac{\sigma_{zz}}{T_z})^2 + (\frac{\sigma_{rz}}{S_{rz}})^2 + (\frac{\sigma_{\theta z}}{S_{\theta z}})^2} = 1, \tag{8}$$

Off-axis failure criterion :

$$\frac{\sigma_p}{\sqrt{(T_r.\overrightarrow{e_1}.\overrightarrow{r})^2 + (T_\theta.\overrightarrow{e_\theta}.\overrightarrow{n})^2 + (T_z.\overrightarrow{e_z}.\overrightarrow{n})^2}} = 1. \tag{9}$$

The use of these criteria, based upon Hashin failure theory [43], was inspired from a previous use in Feerick et al. [44]. Damage initiates when one of the criteria reaches a value of one. Failure in the cylindrical directions was defined by: the radial failure criterion (Eq. 6), the circumferential failure criterion (Eq. 7), and the longitudinal failure criterion (Eq. 8). The parameters T_i and S_{ij} $(i, j \in r, \theta, z)$ define the tensile and shear strengths, respectively. The last failure criterion (Eq. 9) defines the off-axis directions. In this criterion, the principal stress σ_p is divided by a relative contribution of the different tensile strengths. $\overrightarrow{n}$ is the normal vector to the crack surface and $\overrightarrow{e_i}$ $(i, j \in r, \theta, z)$ are the local cylindrical directions at the point. In all criteria, the crack propagates in the plane normal to the direction assigned to the criterion.

The failure criteria were implemented in Abaqus using the FORTRAN user subroutine UDMGINI in conjunction with XFEM to model crack propagation. With this method, the propagation of the tear is computed by incorporating additional enrichment functions to the continuous displacement field to capture the singularity around the crack tip (asymptotic crack tip functions) and the jump in displacement across the crack surfaces (Heaviside jump functions) [45]. The XFEM method was chosen in preference to the cohesive zone method to simulate crack propagation because the location of the crack path is not known *a priori*. A hard contact was defined between the new crack surfaces to avoid intersection of the elements after crack opening. The propagation of the crack was governed by a linear traction-separation law. A scalar damage variable, d, was defined for each failure criterion. This damage parameter is initially set to zero ($d = 0$). Once one of the failure criteria was reached and damage was initiated, the cohesive stiffness was degraded upon further loading until complete freedom of the nodes ($d = 1$). The total energy dissipated during the separation of the surfaces is G_c.

The tensile strengths of the media in the longitudinal and circumferential directions were defined according to Angouras et al. [46]. In this study, they performed tensile tests in different areas of ascending thoracic aortas. The tensile strengths of the right lateral region were used in our study because this is the most common location of aortic dissection [47]. The radial tensile strength and the shear strength of the media in the different directions were taken from Sommer et al. [21] who performed uniaxial tests and triaxial shear tests on aneurysmatic and dissected human thoracic aortas. The standard deviations were used to define the domains of the strength variables in the designs of experiment (Section II-E). These values are reported in Table II. The tensile and shear strengths of the adventitia were considered infinite because aortic dissection propagates only in the medial layer. The fracture energy per reference area G_c was assumed to be 5.0 mJ/cm^2 [23].

Type	Parameters	Medial failure stress (kPa)	Reference
Tensile	T_r	131 ± 56	[21]
	T_θ	1061 ± 128	[46]
	T_z	551 ± 98	[46]
Shear	$S_{r\theta}$	97 ± 6	[21]
	S_{rz}	120 ± 6	[21]
	$S_{\theta z}$	918 ± 313	[21]

TABLE II: Failure parameters of the numerical model (mean ± SD).

D. Finite element simulation

The first step of the simulation consisted in closing the opening angle to obtain a residually stressed model (Figure 3b). Then, the aortic model was stretched axially to account for the axial stretch present *in vivo* in the aorta (Figure 3c) [48], [49]. At this point in the simulation, the unloaded *in vivo* configuration was reached. The initial aortic diameter was recalculated for each simulation to obtain a similar diameter of 20 mm in the *in vivo* configuration. Finally, the aorta was inflated until the crack propagated (Figure 3d). Pressure was also applied to the crack surfaces during inflation. The wall shear stress was neglected in the loading conditions of the model due to its relatively low magnitude compared to the pressure [50]. Concerning the boundary conditions, once the opening angle was closed and the model pre-stretched, the proximal and the distal faces were axially blocked to prevent the aorta from returning to its original position. Radial displacement remained free.

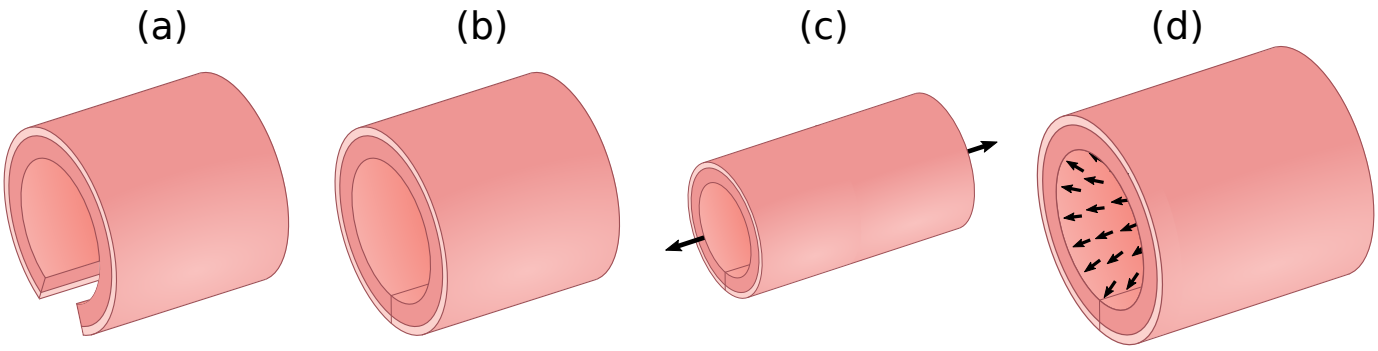

Fig. 3: Sketch of the different steps of the simulation. (a) The two-layer model in the initial state. (b) The residual angle is closed. (c) The axial stretch is applied; the physiological state is reached. (d) The pressure is applied inside the aorta until propagation of the crack.

E. Design of experiment

The influence of different factors on the onset and propagation of aortic dissection was investigated for all three tear configurations. The hyperelastic parameters were kept constant. Three full factorial experimental designs with interactions were performed. The parameters studied were as follows:

- Crack geometrical factors (D the crack depth, L the crack length, W the crack width). Two of the three parameters are studied for each tear configuration according to the plane in which the initial tear is located. They are presented in Figure 1.
- Crack position in the radial direction, defined as P (Figure 1).
- Tensile strength. The parameter range was defined by varying the tensile strengths T_i by ± 2 SD$_i$ with $i = r, \theta, z$ and SD$_i$ the standard deviation of the stress strength value associated in the i direction. The values of the tensile strengths and the associated deviations were chosen according to the literature (Table II).
- Shear strength. The parameter range was defined by varying the shear strengths S_i by ± 2 SD$_i$ with $i = r, \theta, z$ and SD$_i$ the standard deviation of the stress strength value associated in the i direction. The values of the shear strengths and the associated deviations were chosen according to the literature (Table II).
- The opening angle α. The maximum value was chosen according to Saini et al. [51].
- λ, the initial stretch applied to the aorta to account for the physiological stretch. The maximum value was chosen according to Humphrey et al. [38].

Their domains are presented in Table III. The value of two standard deviations was chosen as it includes 95% of the strength values. The tensile and shear strengths were varied as a whole and not per directions to keep the computational time reasonable as a simulation took around one hour to complete on a computer cluster.

The influence of 7 factors were assessed, thus, $2^7 = 128$ simulations were run for each tear orientation. One simulation was added to account for the middle points for each experimental design. The outputs of the simulation were:

	θ-z tear		r-z tear		r-θ tear	
Parameters	Min	Max	Min	Max	Min	Max
Crack depth (mm)	-		0.2	0.72	0.2	0.72
Crack length (mm)	0.5	2.5	0.5	2.5	-	
Crack width (°)	10	60	-		10	60
Crack position (mm)	0.36	1.1	0	0.7	0	0.7
Tensile strength (kPa)	$T-2$ SD	$T+2$ SD	$T-2$ SD	$T+2$ SD	$T-2$ SD	$T+2$ SD
Shear strength (kPa)	$S-2$ SD	$S+2$ SD	$S-2$ SD	$S+2$ SD	$S-2$ SD	$S+2$ SD
Opening angle (°)	0	140	0	140	0	140
Initial stretch (-)	1.0	1.2	1.0	1.2	1.0	1.2

TABLE III: Ranges of the parameters of the numerical model used in the sensitivity study

- The critical pressure at which the tear started to propagate.
- The plane of propagation of the crack, defined by its normalized normal vector with r, θ and z components (e.g. a $[0, 1, 0]$ vector means a propagation in the plane normal to the θ direction). Each component of the vector was taken as an output.

The 4 outputs were computed as a linear combination of the different parameters by fitting a polynomial with the ordinary least squares method for each output. The polynomials were defined by

$$Y = \beta_0 + \sum_{k=1}^{N} \beta_k x_k + \sum_{i,j=1,j>i}^{N} \beta_{ij} x_i x_j \ + \epsilon \qquad i \neq j, \quad (10)$$

where Y is the output, N = 7 is the number of parameters, x is the parameter value in its coded space (between -1 and 1), β reflects its influence (except for β_0), and ϵ is the estimated error.

1) Statistical analysis: A statistical analysis was used to assessed the quality of the fitted response. After ensuring that the residuals followed a normal distribution, an analysis of variance (ANOVA) was performed. The coefficients of determination r^2 were calculated and an F-test was used to evaluate the overall validity of each design of experiment. Finally, the significance of each parameter on the response was assessed using a Student's t-test.

In the DoE, one of the main assumptions is that the response

is linear, which may not be the case with a complex model like the one presented herein. The curvature of the response was tested in each tear configuration using centre points by adding a $\beta_c x_c$ term to the Equation 10 with $x_c = 0$ if a center point is tested and $x_c = 1$ otherwise. Finally, the hypothesis $\beta_c \neq 0$ was tested to investigate the presence of curvature.

III. Results

The simulations of tear propagation were performed and three illustrative results of crack propagation are presented, along with a graph representing the crack surface as a function of the pressure in Figure 4. The crack initiation was caused by stress concentration at the tear site. In the θ-z tear configuration in Figure 4, the crack appears to propagate in the same direction as one of the fibre family as seen in Gültekin et al. [30]. In the r-z tear configuration example, the propagation mainly follows the circumferential direction whereas in the r-θ tear configuration the propagation principally follows the longitudinal direction. The graphs in Figure 4c show that the crack does not propagate linearly but by jumps, before diverging. This is explained by the fact that the model is pressure-controlled, which leads to an instability. As observed experimentally by Roach et al. [52] in a volume-driven study, once the critical pressure is reached, the crack begins to propagate, however, the pressure decreases or remains constant during the propagation.

A. Design of experiment

1) Critical pressure: The mean critical pressures were 206 ± 203 mmHg, 251 ± 152 mmHg, and 239 ± 153 mmHg for the θ-z, r-z, and r-θ tear configurations, respectively. The first-order polynomial coefficients were fitted and are reported in Figure 5 along with the corresponding Pareto curves. The factor interactions are presented in Supplementary Material. The higher the absolute value of the coefficient, the greater the influence of the corresponding parameter on the critical pressure. The F-test probability was inferior to 0.001 for all tear configurations. The r^2 is a measure of how well a model reproduces the observed results. The r^2 were 0.90 for the θ-z tear configuration, 0.95 for the r-z tear configuration, and 0.93 for the r-θ tear configuration. Tensile strength is by far the most influential parameter as it accounts for about 50% of the impact of the parameters on the model response in all tear configurations. Depending on the plane where the initial tear is located, the influential factors differ. The initial stretch is mostly influential in the r-z and r-θ tear cases. The effect of residual stress and shear strength appear to be limited in all three cases as they accounts for less than 10% of the total response.

The curvatures (non-linearities) of the responses were evaluated using centre points and stands in a low range ($p > 0.1$), not compromising the validity of the model. Furthermore, it should be emphasized that the main objective of the study was not to build a response surface of the FE model, but to assess the overall influence and to find the most significant factors in the propagation of a tear.

2) Direction of propagation: Only height simulations propagated normal to an off-axis direction, and in all cases the failure directions were close to one of the cylindrical directions. Thus, the off-axis directions were set to the nearest cylindrical direction. The distributions of the propagation planes are reported in Figure 6 for each tear configuration. In the θ-z tear configuration, 80% of the simulations propagated in the θ-z plane, 6% in the r-z plane, and 14% in the r-θ plane. In the r-z tear configuration, 50% of the simulations propagated in the θ-z plane, 38% in the r-z plane, and 12% in the r-θ plane. In the r-θ tear configuration 45% of the simulations propagated in the θ-z plane, 16% in the r-z plane, and 39% in the r-θ plane.

The first-order polynomial coefficients for each direction of propagation are reported in Figure 7 along with the corresponding Pareto curves, for all three tear cases. The factor interactions are presented in Supplementary Material. For a defined tear configuration, the higher the absolute value of the coefficient, the higher the influence of the corresponding parameter on crack propagation in the plane presented. The F-test probability was inferior to 0.001 for all tear configurations. The increase in tensile strength decreases the risk of crack propagation in the θ-z plane in all three tear configurations. The position of the tear has an influence of about 30% on the probability of propagation of the tear in the θ-z plane only in the θ-z tear configuration. The initial stretch increases the probability of a tear propagating in the r-θ plane from 30% to 40%, for every tear configuration.

IV. Discussion

In the present work, a model for the initiation and propagation of aortic dissection was developed in three tear configurations based on the extended finite element method. The influence of multiple parameters of the model on the critical pressure and plane of propagation was assessed using designs of experiment.

Post-initiation numerical convergence was difficult to achieve due to the unstable nature of crack propagation in soft tissue, along with the nonlinearity of the material. The use of a commercial finite element code (Abaqus/Standard) limits the possibilities to address the convergence issue, e.g. XFEM cannot be used with explicit methods. Therefore, the investigation was limited to the early stages of aortic dissection: the initiation and beginning of tear propagation.

The creation of an intimal tear may be initiated by a fatigue process activated by blood pressure. Hypertension, one of the main risk factors for aortic dissection [1], amplifies this phenomenon. The fatigue process locally decreases the strength of the aortic wall, resulting in the creation of a tear and its propagation along the aorta. The propagation can be triggered by a sudden high blood pressure, e.g. when playing sports [53]. A summary of experimental and numerical data related to critical pressure is given in Table IV. It is generally accepted that pulsatile flow reduces the critical pressure compared to static pressure due to the dependence of critical pressure on $\frac{dP}{dt}_{max}$ [54], [55]. It should be noted that comparison of the studies presented in Table IV is complex due to the differences

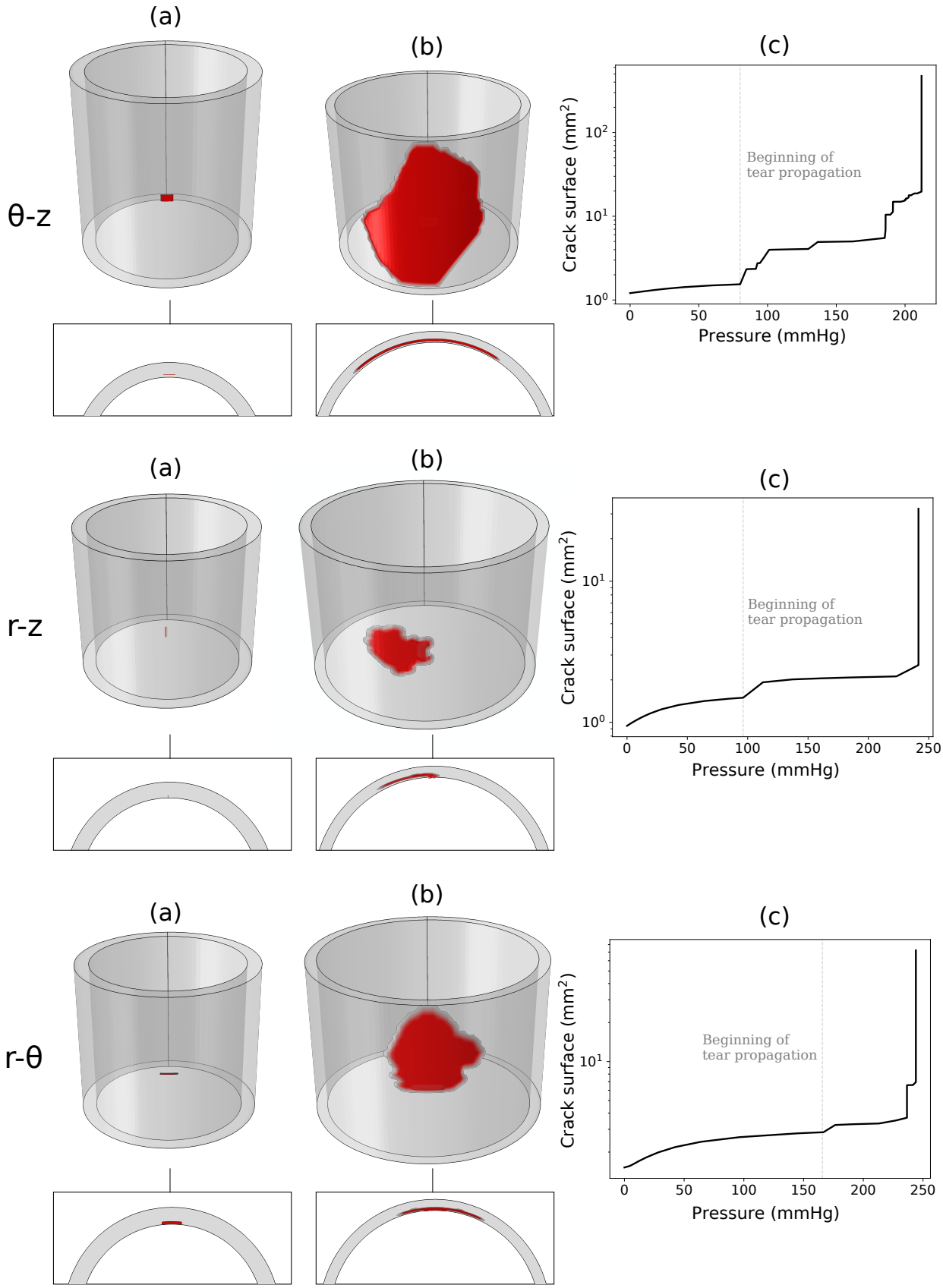

Fig. 4: The evolution of a tear propagation was presented for each tear configuration. A 3-D view and a cross-section view of the aortic wall are presented: (a) in the residually stressed state and (b) after crack propagation. Isosurfaces are used to visualize the crack propagation with $d > 0.5$. (c) A graph representing the crack surface as a function of the pressure is also presented. The y axis is in logarithmic scale.

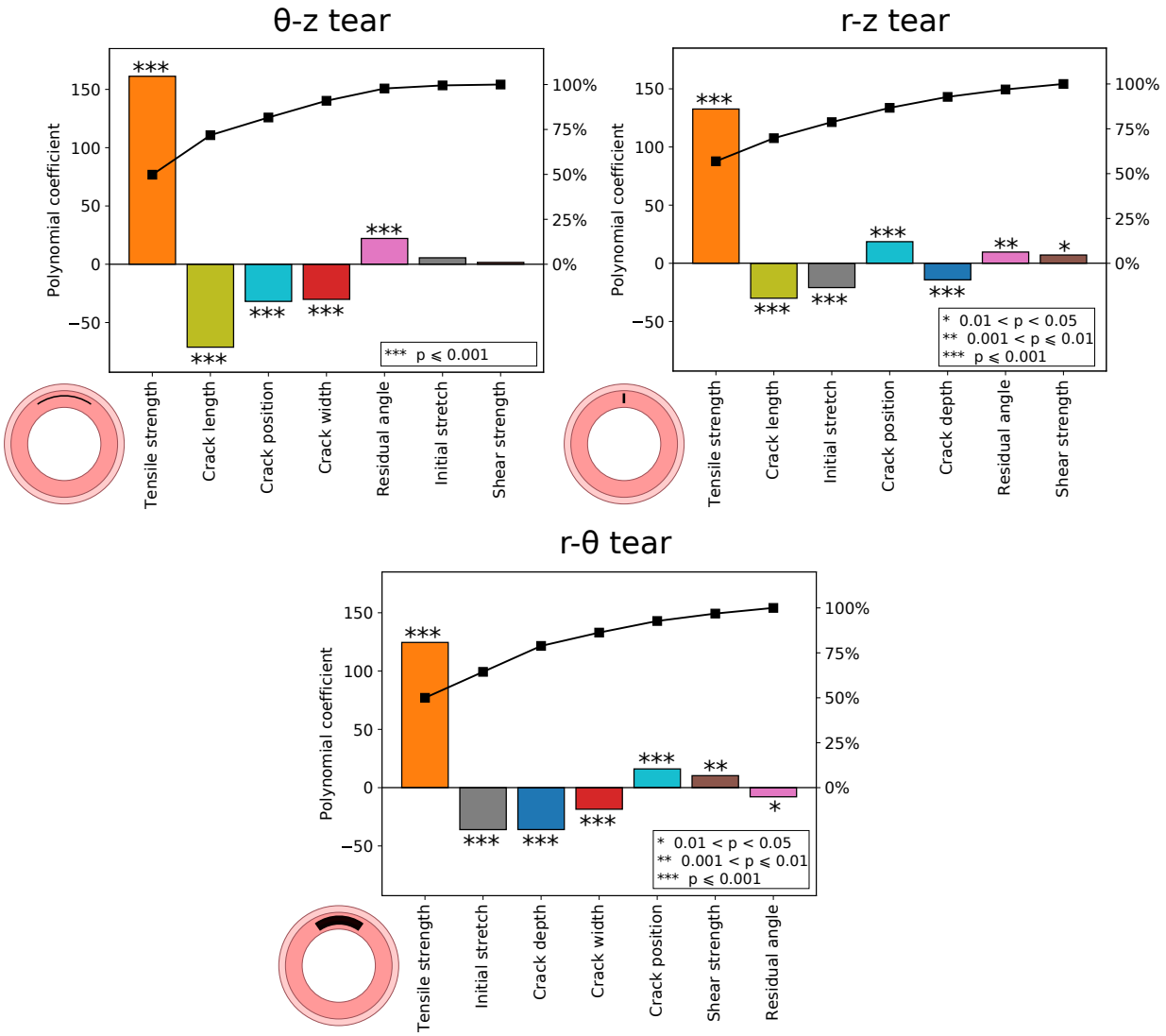

Fig. 5: First-order polynomial coefficients in each tear configuration with the critical pressure as output. The factors are presented in decreasing order in terms of absolute values. For each graph, the Pareto curve is shown in black with the scale on right axis, it represents the cumulative percentage of the parameter influences. The letter p stands for significance.

in techniques and tissues. The mean critical pressures found in the present study are in the experimental range; however, they are lower than the literature values obtained with static pressure. This is certainly due to the fact that the strength values used for the fracture criteria were derived from mechanical tests on diseased aortic tissue. Hence, the results suggest that the critical pressures in a diseased aorta with a tear can be reached under physiological conditions, such as during weight lifting, for example [53], [56]. The most influential factor in reducing the critical pressure is the medial tensile strength, indicating that a medial degeneration is a possible cause for an aortic dissection to occur. The tensile strength also greatly influences the plane of propagation, an impaired media has a higher probability of propagating a tear along the aorta (in the θ-z plane) in all tear configurations (Figure 7). On the other hand, medial shear strength does not significantly affect critical pressure or plane of propagation. This result may be caused by structural effects at the scale of the medial lamellae, which were not taken into account due to the continuous nature of the FE model, as shear fracture (mode II) was identified as a key process in delamination [20], [22]. Haslach et al. [20] suggested that shear stress is strongly related to the lamellar structure of the media due to the relative slip between medial layers. In the present study, the media was modelled by a continuous material without taking into account the medial structure, which may also explain why our model failed to capture the influence of shear strength on tear initiation and propagation.

In their experimental study, Tam et al. [18] observed that a lower pressure was required to propagate a dissection close to the adventitia, confirming that aortic dissection propagates preferentially in the outer third media [60]. The same result was found in our study for the θ-z tear configuration as a result of the stress concentration created by the discontinuity, confirming that non-communicating dissections preferentially occur closer to the adventitia. Furthermore, Figure 7 showed

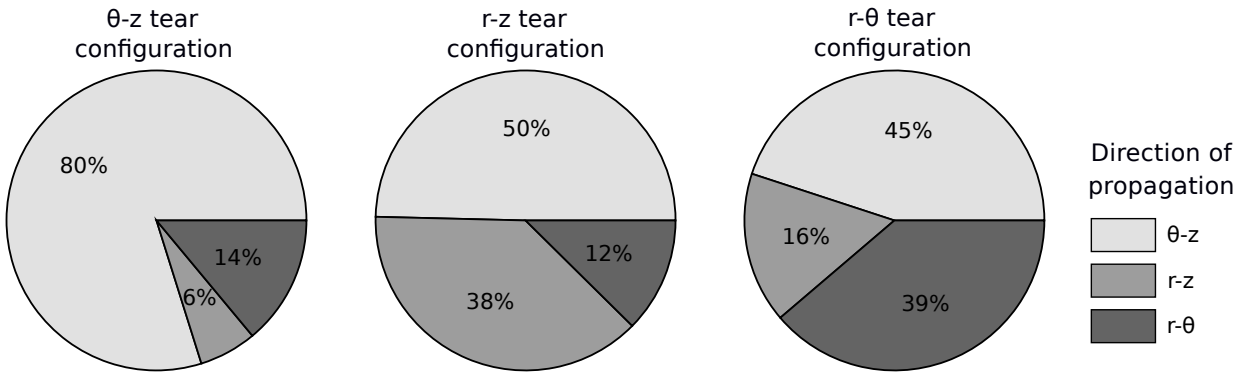

Fig. 6: Distribution of the planes of tear propagation for each tear configuration.

Experimental studies				
Tissue	Flow state	Experimental method	Critical pressure (mmHg)	Reference
Canine descending thoracic aorta	Static	Intramural liquid infusion	472 ± 76	Hirst and Johns [57]
Canine descending thoracic aorta	Pulsatile	Slit intramural bleb followed by inflation	185 (pulse pressure 160)	Prokop et al. [54]
Canine thoracic aorta	Pulsatile (no flow)	Intramural liquid infusion	370 ± 89	Baardwijk et al. [55]
Pig upper descending thoracic aorta	Static	Intramural liquid infusion	579 ± 11	Carson et al. [11]
Human aorta	Static	Intramural liquid infusion	596 ± 214	Tiessen et al. [12]
Canine thoracic aorta	Pulsatile	Aortic pocket followed by inflation	125 (pulse pressure 50)	Mitsui et al. [58]
Porcine lower thoracic aorta	Static	Intramural liquid infusion	854 ± 134	Roach et al. [52]
Porcine lower abdominal aorta	Static	Intramural liquid infusion	634 ± 204	Roach et al. [52]
Porcine thoracic aorta	Static	Slit intramural bleb followed by inflation	306 ± 72	Tam et al. [18]
Porcine thoracic aorta	Pulsatile	Contralateral incisions followed by inflation	152 ± 43	Dziodzio et al. [59]
Descending thoracic porcine aorta	Pulsatile	Creation of dissection on inverted aorta followed by inflation	180 (pulse pressure 200)	Peelukhana et al. [19]
Numerical studies				
Tissue	Flow state	Numerical method	Critical pressure (mmHg)	Reference
Human ascending thoracic aortic aneurysm	Static	Constrained mixture model	263	Mousavi et al. [31]
Human thoracic aorta	Static	Phase-field model	Between 120 and 600 mmHg	Gultekin et al. [30]
Human ascending aorta	**Static**	**XFEM - θ-z tear configuration**	**206 ± 203**	**Present study**
		XFEM - r-z tear configuration	**251 ± 152**	
		XFEM - r-θ tear configuration	**239 ± 153**	

TABLE IV: Critical pressure of aortic tissue in experimental and numerical studies. The critical pressures are presented as mean ± SD.

that the closer the θ-z tear is to the adventitia, the higher the probability of propagating along the aorta (in the θ-z plane). Concerning the r-z and r-θ tear configurations, the position parameter is not relevant as it seems unlikely that a tear appears in either plane without being connected to the lumen.

Geometrical factors are shown to significantly affect critical pressure as demonstrated in Peelukhana et al. [19]. This result was expected as a larger and deeper tear results in higher stress concentrations at the edge of the crack, diminishing the pressure required to initiate a dissection. The length of the crack appears to be the most influential factor among the geometrical factors in the θ-z and r-z tear configurations, whereas in the r-θ tear configuration, it is the depth of the crack. It was also shown that the initial axial stretch decreases the critical pressure in the r-z and r-θ tear configurations. This parameter increases the longitudinal stress in the wall and reduces the amount of stress required to reach the longitudinal tensile strength of the tissue. Increasing the axial stretch also increases the probability of tear propagation in the r-θ plane and, consequently, aortic rupture. On the other hand, the residual stress protects the aorta from tear propagation in the θ-z configuration as the critical pressure increases significantly with the residual stress. The same result was found numerically in Wang et al. [32]. The distribution of directions of propagation (Figure 6) shows that the θ-z plane is predominant in all tear configurations. This means that interlamellar propagation of the tear is the most likely scenario, especially in the θ-z configuration. This result, in agreement with most of clinical observations of extended dissections, can be explained by the low cohesion between the medial lamellae, represented in our model by the low radial cohesive strength [61].

Some limitations to this study should be noted. A stress-based fracture criterion such as the one used in this work is straightforward because it can be determined directly with values from the literature; nevertheless, other formulations might be better suited to heterogeneous anisotropic material

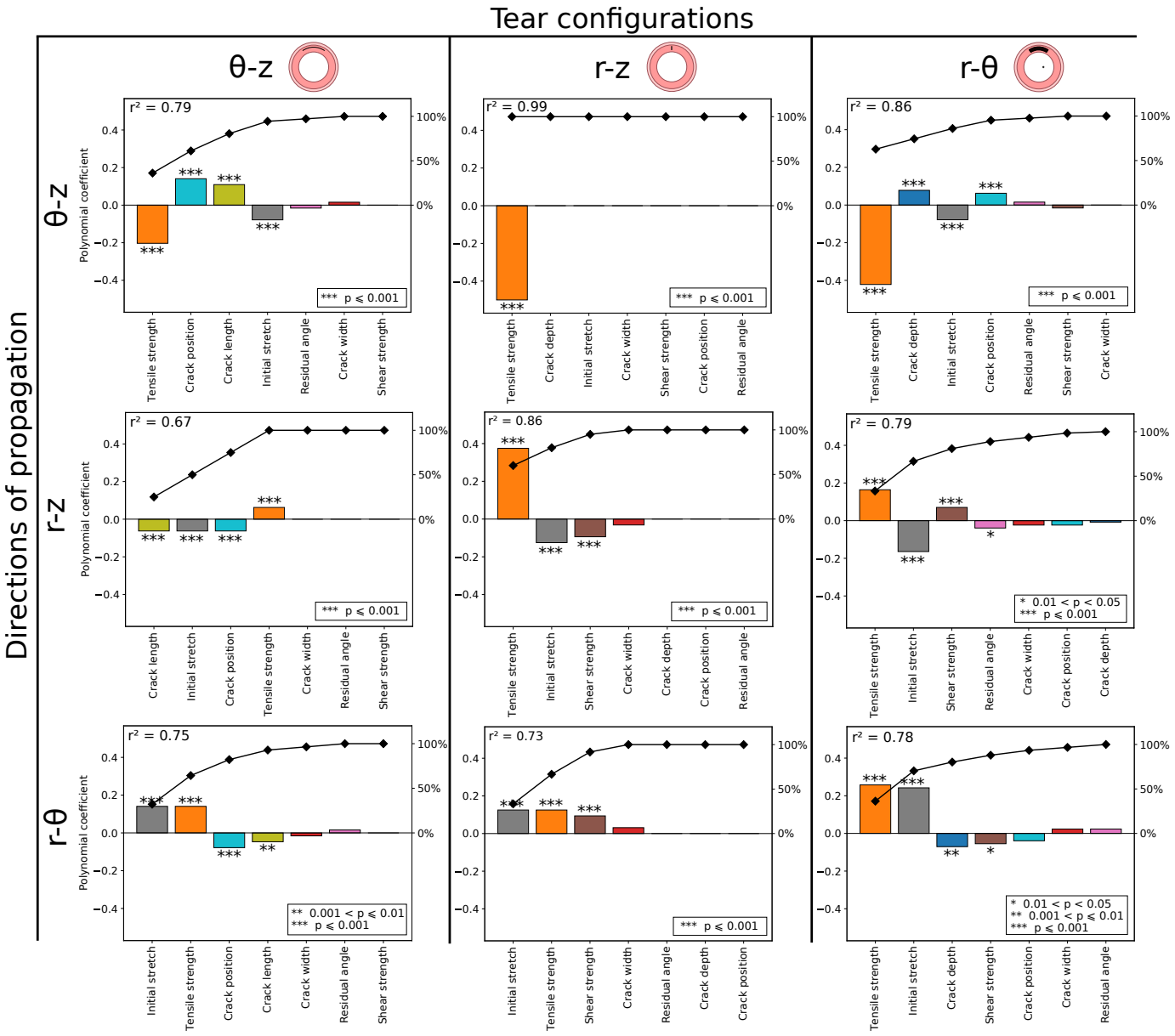

Fig. 7: First-order polynomial coefficients in each tear configuration with the different plane of propagation as outputs. The factors are presented in decreasing order in term of absolute value. For each graph, the Pareto curve is shown in black with the scale on right axis, it represents the cumulative percentage of the parameter influences. The r^2 are shown on the top left corner of each graph. F-test probability <0.001 for all tear configurations. The letter p stands for significance. An example of how to interpret these results: for an initial tear in the θ-z plane, increasing initial stretch increases the likelihood of a propagation in the r-θ (bottom left plot).

such as energy-based criterion [62]. A numerical limitation of this study is the dependence of the results on the domain used for each parameter in the designs of experiments. Soft tissues exhibit a large variability in their mechanical behaviour depending on multiple factors such as, for instance, location, individual, disease. The domains were selected on the basis of experimental investigations from the literature, taking into account the variability of each parameter; however, some limitations should be noted. The domains of the geometrical factors were chosen to investigate the effect of a small tear on the propagation of dissection, although much larger tears were observed in the literature [17]. We assumed that aortic dissection originates from a small tear and that the tear becomes larger with the propagation of the aortic dissection. Another limitation to this work is the assumption that the media is homogeneous when in reality it is not. The medial inner layers differ from the medial outer layers in term of mechanical properties [46]. The location around the aorta also has an influence on the mechanical behaviour [46]. The reason behind these changes is related to local differences in the microstructure. The microstructure plays a key role in the stress distribution along the aorta [63]. In our work, each

layer of the aortic wall was assumed to be homogeneous for simplicity; however, taking into account these local differences seems fundamental in the modelling of a complete dissection along the aorta, especially since the crack path would be influenced by heterogeneities. Other numerical studies investigated the effect of different microstructural components on the mechanical behaviour and fracture of the aortic wall [29], [61], [64]; nevertheless, they did not study the effect of a tear on aortic dissection propagation. Furthermore, surrounding tissues around the aorta were neglected for simplicity in this study, although they may induce pressure on the adventitial side of the aortic wall. Therefore, the internal pressure can be interpreted as a relative pressure equal to the blood pressure applied to the intimal side of the aortic wall minus the pressure induced by the surrounding tissues.

Finally, the main limitation of this study is the lack of validation. The lack of experimental data concerning the investigation of the early stage of aortic dissection is an issue. It can be explained by the difficulties to observe such an event. Nevertheless, the recent developments in imaging techniques may be used to overcome these difficulties and shed light on the early steps of aortic dissection. In addition, this model was used to assess the relative contribution of each factor rather than providing predictive values. In this context, it definitively helps to understand the governing mechanisms of this event. For example, knowing that tensile strength is the main factor contributing to the initiation of dissection (and even more so for θ-z tears) may help with better screening at-risk individuals.

V. Conclusion

Aortic dissection is a complex process involving multiple mechanical factors. The fact that only the final state of the disease is clinically observed hides this complexity. Numerical models can help to understand and quantify the mechanisms involved. The model presented in this study was able to replicate the behaviour of the aorta during the initiation and propagation of an aortic dissection. In addition, different types of tears were compared and the influence of several parameters on the critical pressure and direction of propagation was evaluated with a parametric study for each tear configuration. Although this study remains to be validated with experimental data (on-going research), it provides a better understanding of the mechanisms of aortic dissection propagation. Further studies could investigate and quantify the most influential parameters found in this work in patients suffering from aortic dissection. This could lead to improvements in the detection and treatment of this disease.

Acknowledgements

This work was supported by the European Research Council through Starting Grant AArteMIS n°638804.

References

[1] Christoph A Nienaber, Rachel E Clough, Natzi Sakalihasan, Toru Suzuki, Richard Gibbs, Firas Mussa, Michael P Jenkins, Matt M Thompson, Arturo Evangelista, James SM Yeh, et al. Aortic dissection. *Nat. Rev. Dis. Primers.*, 2(1):1–18, 2016.

[2] Isidre Vilacosta and José Alberto San Román. Acute aortic syndrome. *Heart*, 85(4):365–368, 2001.

[3] MJ Thubrikar, P Agali, and F Robicsek. Wall stress as a possible mechanism for the development of transverse intimal tears in aortic dissections. *J. Med. Eng. Technol.*, 23(4):127–134, 1999.

[4] Christoph A Nienaber, Yskert von Kodolitsch, Ben Petersen, Roger Loose, Udo Helmchen, Axel Haverich, and Rolf P Spielmann. Intramural hemorrhage of the thoracic aorta: diagnostic and therapeutic implications. *Circulation*, 92(6):1465–1472, 1995.

[5] Jae-Kwan Song. Update in acute aortic syndrome: intramural hematoma and incomplete dissection as new disease entities. *J. Cardiol.*, 64(3):153–161, 2014.

[6] Patrick T O'Gara and Roman W DeSanctis. Acute aortic dissection and its variants: toward a common diagnostic and therapeutic approach. *Circulation*, 92(6):1376–1378, 1995.

[7] Albert E Hirst, Varner J Johns, and S Wesley Kime. Dissecting aneurysm of the aorta: a review of 505 cases. *Medicine*, 37(3):217, 1958.

[8] R Erbel, F Alfonso, C Boileau, O Dirsch, B Eber, A Haverich, H Rakowski, J Struyven, K Radegran, U Sechtem, et al. Diagnosis and management of aortic dissection: task force on aortic dissection, european society of cardiology. *Eur. Heart J.*, 22(18):1642–1681, 2001.

[9] Francis Robicsek and Mano J Thubrikar. Hemodynamic considerations regarding the mechanism and prevention of aortic dissection. *Ann. Thorac. Surg.*, 58(4):1247–1253, 1994.

[10] Qingzhuo Chi, Ying He, Yong Luan, Kairong Qin, and Lizhong Mu. Numerical analysis of wall shear stress in ascending aorta before tearing in type a aortic dissection. *Comput. Biol. Med.*, 89:236–247, 2017.

[11] Michael W Carson and Margot R Roach. The strength of the aortic media and its role in the propagation of aortic dissection. *J. Biomech.*, 23(6):579–588, 1990.

[12] IM Tiessen and MR Roach. Factors in the initiation and propagation of aortic dissections in human autopsy aortas. *J. Biomech. Eng.*, 115(1):123–125, 1993.

[13] Christoph A Nienaber and Rachel E Clough. Management of acute aortic dissection. *The LancetBiomech. Model. Mechanobiol.*, 385(9970):800–811, 2015.

[14] Alexander Emmott, Ismaïl El-Hamamsy, and Richard L Leask. Histopathological and biomechanical properties of the aortic wall in 2 patients with chronic type a aortic dissection. *Cardiovasc. Pathol.*, 29:48–52, 2017.

[15] Leslie E Quint, Joel F Platt, Seema S Sonnad, G Michael Deeb, and David M Williams. Aortic intimal tears: detection with spiral computed tomography. *J. Endovasc. Ther.*, 10(3):505–510, 2003.

[16] Masaki Nakashima, Shuichiro Kaji, Ryosuke Murai, Yasuhiro Sasaki, Mitsuhiko Ota, Kitae Kim, Takafumi Yamane, Takeshi Kitai, Atsushi Kobori, Natsuhiko Ehara, et al. Detection of micro intimal tear at a very early stage in patients with acute aortic intramural hematoma. *Circulation*, 134(suppl_1):A13989–A13989, 2016.

[17] Lars G Svensson, Sherif B Labib, Andrew C Eisenhauer, and John R Butterly. Intimal tear without hematoma: an important variant of aortic dissection that can elude current imaging techniques. *Circulation*, 99(10):1331–1336, 1999.

[18] Amy SM Tam, M Catherine Sapp, and Margot R Roach. The effect of tear depth on the propagation of aortic dissections in isolated porcine thoracic aorta. *J. Biomech.*, 31(7):673–676, 1998.

[19] Srikara V Peelukhana, Yanmin Wang, Zachary Berwick, Jarin Kratzberg, Joshua Krieger, Blayne Roeder, Rachel E Cloughs, Albert Hsiao, Sean Chambers, and Ghassan S Kassab. Role of pulse pressure and geometry of primary entry tear in acute type b dissection propagation. *Ann. Biomed. Eng.*, 45(3):592–603, 2017.

[20] Henry W Haslach Jr, Ahmed Siddiqui, Amanda Weerasooriya, Ryan Nguyen, Jacob Roshgadol, Noel Monforte, and Eileen McMahon. Fracture mechanics of shear crack propagation and dissection in the healthy bovine descending aortic media. *Acta Biomater.*, 68:53–66, 2018.

[21] Gerhard Sommer, Selda Sherifova, Peter J Oberwalder, Otto E Dapunt, Patricia A Ursomanno, Abe DeAnda, Boyce E Griffith, and Gerhard A Holzapfel. Mechanical strength of aneurysmatic and dissected human thoracic aortas at different shear loading modes. *J. Biomech.*, 49(12):2374–2382, 2016.

[22] J Brunet, B Pierrat, E Maire, J Adrien, and P Badel. A combined experimental-numerical lamellar-scale approach of tensile rupture in arterial medial tissue using x-ray tomography. *J. Mech. Behav. Biomed. Mater.*, 95:116–123, 2019.

[23] Gerhard Sommer, T Christian Gasser, Peter Regitnig, Martin Auer, and Gerhard A Holzapfel. Dissection properties of the human aortic media: an experimental study. *J. Biomech. Eng.*, 130(2):021007, 2008.

[24] Salvatore Pasta, Julie A Phillippi, Thomas G Gleason, and David A Vorp. Effect of aneurysm on the mechanical dissection properties of the human ascending thoracic aorta. *J. Thorac. Cardiovasc. Surg.*, 143(2):460–467, 2012.

[25] Christopher Noble, Nicole Smulders, Roger Lewis, Matt J Carré, Steve E Franklin, Sheila MacNeil, and Zeike A Taylor. Controlled peel testing of a model tissue for diseased aorta. *J. Biomech.*, 49(15):3667–3675, 2016.

[26] Xiaochang Leng, Boran Zhou, Xiaomin Deng, Lindsey Davis, Susan M Lessner, Michael A Sutton, and Tarek Shazly. Experimental and numerical studies of two arterial wall delamination modes. *J. Mech. Behav. Biomed. Mater.*, 77:321–330, 2018.

[27] T Christian Gasser and Gerhard A Holzapfel. Modeling the propagation of arterial dissection. *Eur. J. Mech. A Solids*, 25(4):617–633, 2006.

[28] A Ferrara and ANNA Pandolfi. A numerical study of arterial media dissection processes. *Int. J. Fract.*, 166(1-2):21–33, 2010.

[29] Siladitya Pal, Alkiviadis Tsamis, Salvatore Pasta, Antonio D'Amore, Thomas G Gleason, David A Vorp, and Spandan Maiti. A mechanistic model on the role of "radially-running" collagen fibers on dissection properties of human ascending thoracic aorta. *J. Biomech.*, 47(5):981–988, 2014.

[30] Osman Gültekin, Sandra Priska Hager, Hüsnü Dal, and Gerhard A Holzapfel. Computational modeling of progressive damage and rupture in fibrous biological tissues: application to aortic dissection. *Biomech. Model. Mechanobiol.*, pages 1–22, 2019.

[31] S Jamaleddin Mousavi, Solmaz Farzaneh, and Stéphane Avril. Computational predictions of damage propagation preceding dissection of ascending thoracic aortic aneurysms. *Int. j. numer. method. biomed. eng.*, 34(4):e2944, 2018.

[32] Lei Wang, Steven M Roper, Nicholas A Hill, and Xiaoyu Luo. Propagation of dissection in a residually-stressed artery model. *Biomech. Model. Mechanobiol.*, 16(1):139–149, 2017.

[33] Lei Wang, Nicholas A Hill, Steven M Roper, and Xiaoyu Luo. Modelling peeling-and pressure-driven propagation of arterial dissection. *J. Eng. Math.*, 109(1):227–238, 2018.

[34] Joseph Brunet, Baptiste Pierrat, and Pierre Badel. Review of current advances in the mechanical description and quantification of aortic dissection mechanisms. *IEEE Rev. Biomed. Eng.*, 2020.

[35] L Cardamone, A Valentin, JF Eberth, and JD Humphrey. Origin of axial prestretch and residual stress in arteries. *Biomech. Model. Mechanobiol.*, 8(6):431, 2009.

[36] Gerhard A Holzapfel, Gerhard Sommer, Martin Auer, Peter Regitnig, and Ray W Ogden. Layer-specific 3d residual deformations of human aortas with non-atherosclerotic intimal thickening. *Ann. Biomed. Eng.*, 35(4):530–545, 2007.

[37] Michel R Labrosse, Eleanor R Gerson, John P Veinot, and Carsten J Beller. Mechanical characterization of human aortas from pressurization testing and a paradigm shift for circumferential residual stress. *J. Mech. Behav. Biomed. Mater.*, 17:44–55, 2013.

[38] Jay D Humphrey and Gerhard A Holzapfel. Mechanics, mechanobiology, and modeling of human abdominal aorta and aneurysms. *J. Biomech.*, 45(5):805–814, 2012.

[39] Hannah Weisbecker, David M Pierce, Peter Regitnig, and Gerhard A Holzapfel. Layer-specific damage experiments and modeling of human thoracic and abdominal aortas with non-atherosclerotic intimal thickening. *J. Mech. Behav. Biomed. Mater.*, 12:93–106, 2012.

[40] A Gerhard Holzapfel. *Nonlinear solid mechanics II*. John Wiley & Sons, Inc., 2000.

[41] Gerhard A Holzapfel, Thomas C Gasser, and Ray W Ogden. A new constitutive framework for arterial wall mechanics and a comparative study of material models. *J. Elast.*, 61(1-3):1–48, 2000.

[42] T Christian Gasser, Ray W Ogden, and Gerhard A Holzapfel. Hyperelastic modelling of arterial layers with distributed collagen fibre orientations. *J. R. Soc. Interface*, 3(6):15–35, 2006.

[43] Zvi Hashin. Failure criteria for unidirectional fiber composites. *J. Appl. Mech.*, 47(2):329–334, 1980.

[44] Emer M Feerick, Xiangyi Cheryl Liu, and Patrick McGarry. Anisotropic mode-dependent damage of cortical bone using the extended finite element method (xfem). *J. Mech. Behav. Biomed. Mater.*, 20:77–89, 2013.

[45] Ted Belytschko and Tom Black. Elastic crack growth in finite elements with minimal remeshing. *Int. J. Numer. Methods Eng.*, 45(5):601–620, 1999.

[46] Dimitrios C Angouras, Eleftherios P Kritharis, and Dimitrios P Sokolis. Regional distribution of delamination strength in ascending thoracic aortic aneurysms. *J. Mech. Behav. Biomed. Mater.*, 2019.

[47] William C Roberts. Aortic dissection: Anatomy, consequences, and causes. *Am. Heart J.*, 101(2):195 – 214, 1981.

[48] JD Humphrey, JF Eberth, WW Dye, and RL Gleason. Fundamental role of axial stress in compensatory adaptations by arteries. *J. Biomech.*, 42(1):1–8, 2009.

[49] Stéphane Avril, Pierre Badel, Mohamed Gabr, Michael A Sutton, and Susan M Lessner. Biomechanics of porcine renal arteries and role of axial stretch. *J. Biomech. Eng.*, 135(8), 2013.

[50] Alex J Barker, Craig Lanning, and Robin Shandas. Quantification of hemodynamic wall shear stress in patients with bicuspid aortic valve using phase-contrast mri. *Annals of biomedical engineering*, 38(3):788–800, 2010.

[51] Ashish Saini, Colin Berry, and Stephen Greenwald. Effect of age and sex on residual stress in the aorta. *J. Vasc. Res.*, 32(6):398–405, 1995.

[52] Margot R Roach and SH Song. Variations in strength of the porcine aorta as a function of location. *J. Clin. Invest.*, 17(4):308, 1994.

[53] I Hatzaras, M Tranquilli, M Coady, PM Barrett, Jesse Bible, and JA Elefteriades. Weight lifting and aortic dissection: more evidence for a connection. *Cardiology*, 107(2):103–106, 2007.

[54] Edward K Prokop, Roger F Palmer, and MYRON W WHEAT Jr. Hydrodynamic forces in dissecting aneurysms: in-vitro studies in a tygon model and in dog aortas. *Circ. Res.*, 27(1):121–127, 1970.

[55] Charles van Baardwijk and Margot R Roach. Factors in the propagation of aortic dissections in canine thoracic aortas. *J. Biomech.*, 20(1):67–73, 1987.

[56] C Mayerick, F Carré, and J Elefteriades. Aortic dissection and sport: physiologic and clinical understanding provide an opportunity to save young lives. *J. Card. Surg.*, 51(5):669–681, 2010.

[57] Albert E Hirst Jr and Varner J Johns Jr. Experimental dissection of media of aorta by pressure: its relation to spontaneous dissecting aneurysm. *Circ. Res.*, 10(6):897–903, 1962.

[58] Hideya Mitsui, Hatsuzo Uchida, and Shigeru Teramoto. Correlation between the layer of an intimal tear and the progression of aortic dissection. *Acta Med. Okayama*, 48(2):93–99, 1994.

[59] Tomasz Dziodzio, Andrzej Juraszek, David Reineke, Hansjörg Jenni, Etienne Zermatten, Daniel Zimpfer, Martin Stoiber, Verena Scheikl, Heinrich Schima, Michael Grimm, et al. Experimental acute type b aortic dissection: different sites of primary entry tears cause different ways of propagation. *Ann. Thorac. Surg.*, 91(3):724–727, 2011.

[60] Hiroaki Osada, Masahisa Kyogoku, Motonori Ishidou, Manabu Morishima, and Hiroyuki Nakajima. Aortic dissection in the outer third of the media: what is the role of the vasa vasorum in the triggering process? *Eur. J. Cardio-Thorac. Surg.*, 43(3):e82–e88, 2012.

[61] Colleen M Witzenburg, Rohit Y Dhume, Sachin B Shah, Christopher E Korenczuk, Hallie P Wagner, Patrick W Alford, and Victor H Barocas. Failure of the porcine ascending aorta: multidirectional experiments and a unifying microstructural model. *J. Biomech. Eng.*, 139(3), 2017.

[62] Osman Gültekin, Hüsnü Dal, and Gerhard A Holzapfel. Numerical aspects of anisotropic failure in soft biological tissues favor energy-based criteria: A rate-dependent anisotropic crack phase-field model. *Computer methods in applied mechanics and engineering*, 331:23–52, 2018.

[63] Cristina Cavinato, Jerome Molimard, Nicolas Curt, Salvatore Campisi, Laurent Orgéas, and Pierre Badel. Does the knowledge of the local thickness of human ascending thoracic aneurysm walls improve their mechanical analysis? *Front. bioeng. biotechnol.*, 7:169, 2019.

[64] Sara Roccabianca, Gerard A Ateshian, and Jay D Humphrey. Biomechanical roles of medial pooling of glycosaminoglycans in thoracic aortic dissection. *Biomech. Model. Mechanobiol.*, 13(1):13–25, 2014.